NANO LETTERS

Letter

pubs.acs.org/NanoLett

Reversible Control of Interfacial Magnetism through Ionic-Liquid-Assisted Polarization Switching

Andreas Herklotz,[†] Erjia Guo,[‡] Anthony T. Wong,[†] Tricia L. Meyer,[†] Sheng Dai,[‡] T. Zac Ward,[†] Ho Nyung Lee,*[,†] and Michael R. Fitzsimmons*[,‡]

[†]Materials Science and Technology Division, [‡]Quantum Condensed Matter Division, and [§]Chemical Sciences Division, Oak Ridge National Laboratory, Oak Ridge, Tennessee 37831, United States

ABSTRACT: The ability to control magnetism of materials via electric field enables a myriad of technological innovations in information storage, sensing, and computing. We use ionic-liquid-assisted ferroelectric switching to demonstrate reversible modulation of interfacial magnetism in a multiferroic heterostructure composed of ferromagnetic (FM) $La_{0.8}Sr_{0.2}MnO_3$ and ferroelectric (FE) $PbZr_{0.2}Ti_{0.8}O_3$. It is shown that ionic liquids can be used to persistently and reversibly switch a large area of a FE film. This is a prerequisite for polarized neutron reflectometry (PNR) studies that are conducted to directly probe magnetoelectric coupling of the FE polarization to the interfacial magnetization.

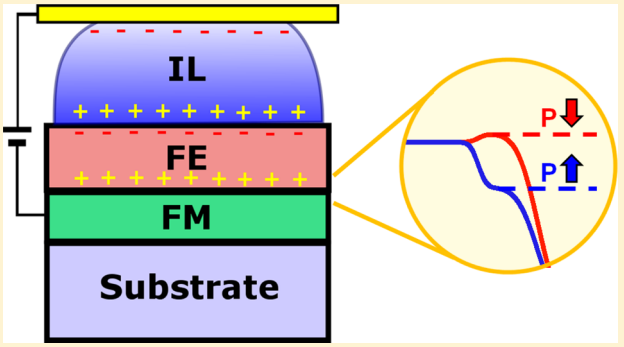

KEYWORDS: *Magnetoelectric coupling, polarized neutron reflectometry, ionic liquid gating, ferroelectric field effect, strongly correlated oxide*

A great deal of work has been devoted to the study of the coupling between ferromagnetic (FM) films, such as the strongly correlated oxide $La_{1-x}Sr_xMnO_3$ (LSMO), and highly polar ferroelectric (FE) films, such as $PbTi_{1-x}Zr_xO_3$ (PZT). It has been shown that the physical properties of LSMO can be significantly affected by a neighboring FE layer,[1−5] an effect that has mainly been attributed to polarization-induced carrier modulation at the FM−FE interface and has consequently been addressed as FE gating.[6,7] For example, reversing the FE polarization of a PZT layer away from the FM−FE interface increases the FM Curie temperature (T_c) and reduces the saturation moment (M_s) of a LSMO film.[8−10] In this scenario, a polarization directed away from the FE−FM interface is believed to induce hole accumulation in a region of the LSMO layer close to the FE−FM interface, which drives the magnetic and electronic structures to higher doping regime in the LSMO phase diagram. However, most studies rely on conventional bulk measurement techniques to characterize the overall properties of the films, which greatly limit our ability to quantify the depth of interaction actually occurring at these interfaces. Thus, direct probing of the interfacial magnetism is greatly needed to clearly understand the magnetoelectric coupling phenomenon at the FE−FM interface. Polarized neutron reflectometry (PNR) is a prime example of a technique that enables determination of magnetic depth profiles with nanometer resolution and, thus, is ideally suited to study the interfacial magnetism affected by the ferroelectric polarization and the spatial extent of the affected region. However, the use of PNR has been limited by the need for large area samples (at least several tens of square millimeters) that preclude stable FE switching.[11] Our recent study used a series of heterostructures in which the FE's polarization was set in the as-grown state without switching, demonstrating the PNR's capability in obtaining depth profiling of magnetization in a heterostructure and the important role of the FE polarization in controlling interfacial magnetization.[12] However, we had to use multiple samples to comparatively understand the interfacial behavior, and thus, there is still a lack of systematic understanding of the interfacial coupling from a single sample without imposing any extra contributions.

In this article, we present a new approach to study the magnetoelectric coupling at the interface of FM and FE layers by the use of ionic liquids (IL). The advantages of IL gating for switching the FE polarization include (1) switching of a large area of a FE thin film that otherwise cannot be accomplished by conventional metallic top electrodes due to shorting via pinholes or other defects; (2) application to very thin FE films, where strong leakage currents would usually impede the application of a bias that is large enough to induce polarization reversal; and (3) switching can be performed in situ on the same sample so that ambiguities arising from the self-poling of differently prepared samples are moot. Here, we use PNR to conclusively confirm that the interfacial magnetization in a FM layer can be enhanced or reduced via IL-assisted FE gating with a FE layer depending on the FE polarization direction.

Received: November 29, 2016
Revised: January 26, 2017
Published: February 1, 2017

DOI: 10.1021/acs.nanolett.6b04949
Nano Lett. XXXX, XXX, XXX−XXX

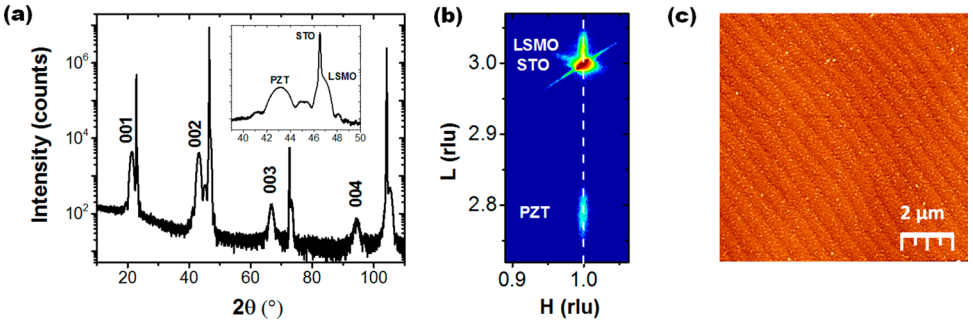

Figure 1. Structural characterization: (a) XRD 2θ–θ scan of a PZT–LSMO heterostructure on a (001) STO substrate. The reflections of the PZT layer are indexed. The inset shows a more detailed scan around the 002 reflection of the heterostructure. (b) Reciprocal space map around the 103 reflection of the heterostructure. The dashed vertical line illustrates the coherent growth of the LSMO–PZT bilayer structure on STO. (c) Topographic AFM image, exhibiting a flat surface with well-defined step-terrace features.

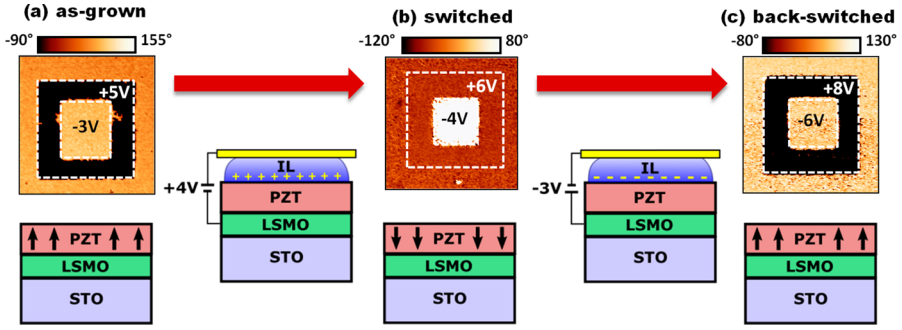

Figure 2. Orientation of the FE polarization and schematic illustration of IL-assisted switching: (a) As-grown PZT film with the self-poled polarization. The phase-contrast PFM image demonstrates that the polarization is pointing upward. (b) The polarization is switched downward by applying +4 V to the IL. (c) Application of −3 V to the IL switches the polarization back to the original upward state. All PFM images are scans on a 3×3 μm^2 large area. The voltages applied to the PFM tip to write upward and downward polarized areas are given inside the boxes. The scales of the PFM phase are shown above the images for each measurement.

Heterostructures of $PbZr_{0.2}Ti_{0.8}O_3$ (~8 nm)–$La_{0.8}Sr_{0.2}MnO_3$ (~12 nm) were grown on (001) $SrTiO_3$ (STO) substrates. Details on sample synthesis can be found elsewhere.[12,13] X-ray diffraction confirms that the films are of high structural quality, f1 phase-pure, epitaxial and fully *c*-axis-oriented (see Figure 1a). Reciprocal space mapping shows that both the LSMO and the PZT layers are coherently strained to the STO substrate (Figure 1b). Step-by-step atomic force microcopy (AFM) measurements done for individual layers show atomically flat surfaces on both LSMO and PZT layers with pronounce step-terrace features, which are critical to induce uniform interfacial modification (see Figure 1c for an example).

To show reversible control of the polarization direction of PZT, the heterostructure was interfaced with the IL 1-ethyl-3-methylimidazolium bis(trifluoromethanesulfonyl)imide or in short Emim-TFSI, an IL that is widely used and well-studied in electric double layer switching experiments.[14] The experiment f2 is illustrated in Figure 2. Figure 2a shows the phase contrast of a piezoresponse force microscopy (PFM) measurement on the as-grown film. The image demonstrates that after growth the film stabilizes in a single-domain self-poled state with an upward FE polarization. This self-poling behavior is in agreement with previous studies.[15] In the next step, the film was contacted with the IL and a bias of +4 V was applied between the LSMO film and the IL. After the bias was applied for 30 min, the IL was removed to determine the polarization state of the PZT film. The PFM image in Figure 2b clearly confirms that the polarization is fully reversed (or points toward the FE–FM interface) compared to the as-grown state. It is important to note that this state was stable without backswitching at least for 2 days as we confirmed with PFM measurements. The polarization switching was fully reversible by applying a bias of opposite sign. Figure 2c demonstrates that the PZT film is reversibly polarized upward after applying a bias of −3 V.

PNR was used to observe the magnetic and structural responses at the PZT–LSMO interface under different FE poled states. Note that PNR requires a large sample area (typically >5 × 5 mm^2) to provide a sufficiently strong neutron signal to generate robust magnetic depth profiles. In PNR, the specular reflectivity is measured as a function of the wave vector transfer Q, with the neutron beam polarization oriented parallel (R^+) and antiparallel (R^-) to an external magnetic field H. The neutron scattering cross-section or neutron scattering length density (SLD) includes contributions from the nuclear (nSLD) and magnetic components (mSLD) of the sample. The variation of R expressed by the spin asymmetry, $SA = (R^+ - R^-)/(R^+ + R^-)$, enables extraction of the magnetization depth profile in the case of specular PNR. The magnetic SLD profiles of the heterostructure are obtained by a model fitting approach with data from both the X-ray reflectivity (XRR), which is sensitive to just the chemical structure, and the PNR. Figure 3a f3 shows XRR data and the best fit for the as-grown film. The resultant depth-dependent nSLD is shown in the top panel of Figure 3d. The XRR for the switched and back-switched state are virtually identical, which demonstrates the robustness of the fitting approach and further indicates that using the IL to switch the film does not lead to noticeable deterioration of the film. In

DOI: 10.1021/acs.nanolett.6b04949
Nano Lett. XXXX, XXX, XXX–XXX

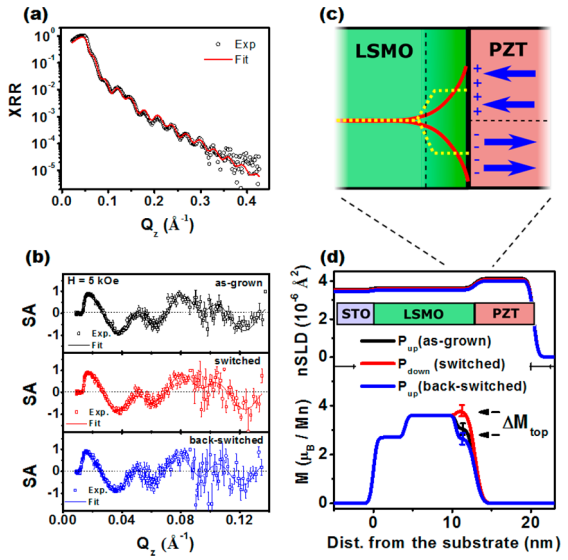

Figure 3. Determination of the chemical and magnetic depth profiles: (a) XRR curve and fit of the as-grown sample. (b) PNR spin-asymmetry (SA) data for the as-grown, switched and back-switched states measured at 5 kOe. (c) Schematic illustration of the FE-polarization-induced hole accumulation and depletion at the FM−FE interface and its effect on the magnetization. The red solid lines illustrate a physical realistic enhancement/reduction of the magnetization near the interface, while the dashed yellow lines are for the step-like approximation used in the simulations. (d) Final neutron scattering length density (nSLD) and magnetization (M) profiles for the three different states. The error bars for the magnetization of the top LSMO layer (ΔM_{top}) are shown to demonstrate that the ferroelectric field effect is larger than the statistical fitting error.

a second step, the nuclear SLD information was used to fit the PNR data with the magnetic SLD as the only part allowed to vary. Figure 3b shows the PNR SA data and the best fits for the as-grown, IL-switched, and back-switched films. The PNR data was recorded at H = 5 kOe and T = 10 K. The magnetization depth profiles are shown in the bottom panel of Figure 3d.

We have found that in all three states, the magnetic behavior of the LSMO layer is best described by three sublayers, where the middle part reflects the bulk behavior of the film and the top and bottom part have a different magnetization presumably due to interface effects with the PZT film and STO substrate, respectively. The observation of a reduced magnetization near interfaces or surfaces has been reported before[16,12,17] and ties to the well-known dead layer phenomenon for ultrathin Manganite films.[18−22] When the polarization points away from the FE−FM interface (i.e., up), the magnetization at the interface is reduced compared to the noninterface regions of the film. When the polarization points toward the FE−FM interface (i.e., down, yielding a hole-depleted state), the magnetization is enhanced beyond the bulk value of the film. The ferroelectric field effect enhances or reduces the magnetization near the FE−FM interface depending on the polarization direction (Figure 3c). The influence of polarization on the magnetism affects the region of the LSMO film within the first couple of unit cell near the FE−FM interface (red solid line of Figure 3c). The data can be adequately explained using a model that approximates the interfacial magnetism by an interfacial layer with constant magnetization and a transition to the bulk magnetization of the film (yellow dashed line).

Our PNR results conclusively reveal that the interfacial magnetism can be reversibly controlled by the polarization direction of the ferroelectric PZT layer and is not the result of chemical effects at the interface. For the as-grown state (black line, P pointing away from the FE−FM interface) the magnetization is reduced as compared to the bulk part of the film, while in the IL switched state (red line, P pointing toward the FE−FM interface), the magnetization not only increases but also exceeds the bulk value. Our fits reveal that the magnetization of the interface layer differs by about ΔM_{top} = 0.7 ± 0.3 μ_B per unit cell for the two polarization states. The uncertainty represents the robustness of the model to the data. The changes to the interface magnetism due to the polarization switching are reversible. After the FE was switched back to the upward-poled state (blue line), the interfacial magnetization is again reduced below the bulk value.

In addition to the PNR experiment, we have used a superconducting quantum interference device (SQUID) magnetometer to measure the total magnetization M of the LSMO film. Figure 4 shows M as a function of temperature

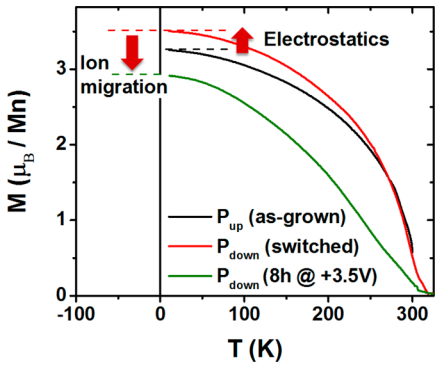

Figure 4. Temperature-dependent SQUID magnetometry data: The total magnetization of an LSMO film in the switched state is enhanced as compared to the as-grown state due to enhanced magnetism at the PZT−LSMO interface. After the application of a positive IL gate bias of 3.5 V for 8 h, the magnetization is reduced below the as-grown state and the ferromagnetic character of the LSMO layer is suppressed. This is typical for oxygen-deficient films and indicates severe ion migration.

during field cooling in 0.1 T for three different states. The data shows that the curves are relatively similar in shape for the as-grown state and the switched state with a small enhancement (~7%) in the switched film. This increase in the low-temperature magnetization is in excellent agreement with the PNR results that suggest enhanced interfacial magnetism due to electrostatic effects induced by the ferroelectric. Note that SQUID magnetometry alone is insufficient to study interfacial effects because changes in the bulk magnetization of the film cannot be excluded.

Studies on IL-switched LSMO without an intermediate Fe layer have suggested that the electric field created at IL interfaces is large enough to potentially induce ion migration.[23] In particular, the generation of oxygen vacancies may alter the electronic and magnetic properties. To address this issue, we applied a positive IL gate bias to a switched PZT−LSMO film for a prolonged period (8 h versus ~10s for normal ferroelectric switching) and compared the magnetic properties to those of a switched film. The temperature-dependent M curve (green) in Figure 4 shows that the ferromagnetic character of the LSMO is suppressed and the total magnet-

DOI: 10.1021/acs.nanolett.6b04949
Nano Lett. XXXX, XXX, XXX−XXX

ization at low temperatures is reduced. This behavior is typical for oxygen-deficient films and indicates that ion migration suppresses the magnetic properties of LSMO films.[23] However, it is important to note that after the application of the positive bias for only a short period (switched state), the opposite effect was observed, and the total magnetization was enhanced. This observation clearly shows that electrostatics is the dominant contribution controlling the interfacial magnetism in the PZT−LSMO heterostructure.

This work demonstrates that for polarization pointing toward the FE−FM interface the magnetization of the 2 nm region of the LSMO layer closest to the interface increases compared to the same region when the polarization points away from the FM−FE interface for the same sample. Our results are consistent with previous theoretical and experimental work.[9,12,24,25] These reports suggest that, in a PZT−LSMO heterostructure, an upward polarization of the PZT layer induces hole accumulation in a thin interfacial LSMO layer, which leads to a reduction in the magnetic moment. A downward polarization has the opposite effect and induces an enhanced moment through hole depletion. Interestingly, the ΔM_{top} = 0.7 μ_B/u.c. in the approximately 2 nm thick interface layer is equal to a switchable magnetic moment of 3.6 μ_B if the electrostatic doping is thought to only affect the first unit cell of LSMO at the FE−FM interface. This value is remarkably close to the bulk moment of LSMO and is in agreement with first-principle calculations, which predict an antiferromagnetic alignment in the first two unit cell of $La_{0.7}Sr_{0.3}MnO_3$ for an upward polarization, while normal ferromagnetic alignment is predicted for a downward polarization.[26,27] It is also interesting to note that the observed behavior is contrary to various previous publications in which an increase of the total magnetization was reported for LSMO films interfaced with PZT layers.[5,28,29] This contradiction can simply be explained with the fact that capping effects dominate over the FE field effect and thus mask the reduction of the magnetization at the FM−FE interface due to electrostatic doping. It also underscores the importance of our depth-sensitive and reversibly PNR study that allows us to separate FE field effects from other influences.

FE gating is expected to not only affect the magnetic properties but also to lead to a modulation of the resistance of the interfacial LSMO layer. Thus, transport measurements can provide further confirmation of the magnetoelectric coupling. We have recorded the change of the resistance of the LSMO layer upon switching a part of the PZT film by applying U_g to the IL. A schematic of the measurement setup is shown in Figure 5a, and details are given in the experimental section. Figure 5b shows the change of the resistance R with respect to the average resistance R_{avg}. We find a clear hysteresis loop with well separated up- and down-poled states. Interestingly, the hysteresis loop is slightly asymmetric, and the switching voltages are almost identical to the ones found by the standard ferroelectric hysteresis loop measured with a small Pt electrode on a slightly thicker (19 nm) PZT film (dashed red curve). We take this as a strong indication that the polarization switching of the PZT is the reason for the observed resistance modulation. It is also a clear confirmation of magnetoelectric coupling. The observed resistive switching is fundamentally different from IL-switched LSMO films without an intermediate FE layer.[23] This further indicates that the FE layer is an effective buffer to reduce ion migration and allows access to pure electrostatic effects.[30−32]

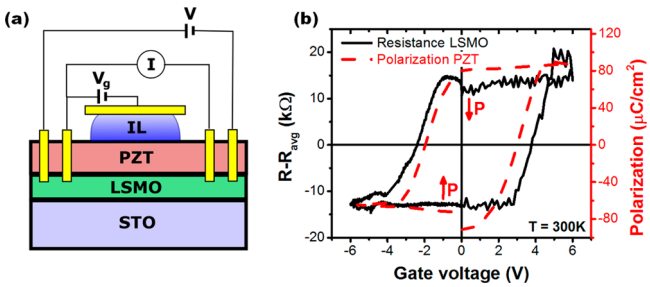

Figure 5. Setup (four-probe) for IL-gated ferroelectric field effect measurements: (a) schematic of the LSMO transport measurement as a function of the gate voltage V_g applied to the IL. (b) Resistance modulation as a function of V_g. The resistance change resembles the ferroelectric hysteresis loop of the PZT layer recorded by a normal P−V measurement (dashed red curve).

In summary, we present a new approach to directly probe the effect of electrostatic doping on the magnetism at a FM/FE interface. We have shown that an IL can be used to reversibly switch the polarization of large areas of PZT films in contrast to standard switching techniques. The in situ switching of whole films allowed us to observe the influence of different electric polarization states of the FE on the interface magnetism in the same sample. It is conclusively shown that the hole accumulation and depletion induced by the FE polarization leads to a reduction and an enhancement of the magnetization in an interface region of a FM LSMO layer, respectively. This finding was supported by transport measurements, revealing a large modulation of the electronic resistance. Our work, thus, presents direct and unambiguous evidence of a controlled interfacial magnetic moment through electrostatic doping via IL-assisted FE gating and opens the path to a better understanding of magnetoelectric coupling phenomena.

Methods. *Film Growth and Characterization.* PZT/LSMO heterostructures were grown on (001)-oriented STO single crystals by pulsed laser deposition. The STO substrates have been chemically treated with buffered HF and were subsequently annealed to achieve a TiO_2-terminated surface. Details of the growth are reported elsewhere.[5] Structural characterization and XRR measurements were carried out with a Panalytical X'Pert MRD four-circle X-ray diffractometer. The total magnetization was measured with a Quantum Design SQUID-VSM instrument. The morphologies of the films were checked with a Nanoscope III AFM. It was also used to record PFM images. The amplitude was set to 0.4 V. Ferroelectric polarization measurements were conducted with an aixACCT TF 2000 Analyzer on thin film capacitor structures with Pt top electrodes of about 5000 μm^2 area. A positive-up negative-down (PUND)-type voltage profile has been used. The PUND-type measurement allows for the accurate determination of a switchable polarization by separating nonswitchable polarization and leakage current contributions.

IL-Assisted Switching. The Emim-TFSI was dried before the use to remove any water contamination. For the PNR experiment, the switching of PZT via IL gating was carried out in ambient conditions immediately after taking the IL out of the drybox. Tissue paper was used to soak up the IL and contact the sample surface in a controllable way. The tissue also served as buffer to avoid direct contact of the top electrode (aluminum foil) with the sample surface. After switching, the samples were ultrasonically cleaned in acetone, methanol, and deionized water to remove the IL. For the transport

DOI: 10.1021/acs.nanolett.6b04949
Nano Lett. XXXX, XXX, XXX−XXX

measurements, the switching of the PZT layer was carried out in a purged and evacuated Quantum Design PPMS chamber.

Polarized Neutron and X-ray Reflectometry. The PNR data was recorded at the BL-4A beamline of the Spallation Neutron Source (SNS) at Oak Ridge National Laboratory. All data were collected at a temperature of 10 K, well below the T_c of LSMO, and under field-cool conditions with an applied magnetic field of 1 T. The XRR measurement was done at room temperature with a Panalytical X'Pert MRD diffractometer. The PNR and XRR data were simulated and fitted with GenX software.[33] The minimum thickness to individual layers was constrained to be 1 nm, a reasonable constraint given the range of Q measured.

Transport Measurements. The transport measurements were conducted at room temperature in zero magnetic fields. Analogous to the ferroelectric polarization measurement, a PUND profile was applied to V_g to determine the resistance change induced by the ferroelectric switching of PZT. By subtracting the up from the positive resistance and the down from the negative resistance, possible contributions due to IL electrostatic effects or leakage currents were eliminated. The hysteresis loop was recorded at a slow rate (approximately 20 min per loop) to reduce the FE switching current that could add to I as well and affect the resistance hysteresis loop.

AUTHOR INFORMATION

Corresponding Authors

*E-mail: hnlee@ornl.gov.

*E-mail: fitzsimmonsm@ornl.gov.

ORCID

Andreas Herklotz: 0000-0002-1545-131X

Sheng Dai: 0000-0002-8046-3931

Notes

The authors declare no competing financial interest.

ACKNOWLEDGMENTS

This work was supported by the U.S. Department of Energy (DOE), Office of Science, Basic Energy Sciences (BES), Materials Sciences and Engineering Division (synthesis and ferroelectric and magnetic characterization) and by the Laboratory Directed Research and Development Program of Oak Ridge National Laboratory (ORNL), managed by UT-Battelle, LLC, for the U.S. Department of Energy (ionic gating and PNR). The use of PNR and piezoresponse force microscopy were performed as user projects at the Spallation Neutron Source and the Center for Nanophase Materials Sciences, respectively, which are sponsored at ORNL by the Scientific User Facilities Division, BES, U.S. DOE.

REFERENCES

(1) Inoue, I. H. *Semicond. Sci. Technol.* **2005**, *20*, S112.

(2) Wen, Z.; Li, C.; Wu, D.; Li, A.; Ming, N. *Nat. Mater.* **2013**, *12*, 617.

(3) Thiele, C.; Doerr, K.; Schultz, L.; Beyreuther, E.; Lin, W.-M. *Appl. Phys. Lett.* **2005**, *87*, 162512.

(4) Wu, S. M.; Cybart, S. A.; Yi, D.; Parker, J. M.; Ramesh, R.; Dynes, R. C. *Phys. Rev. Lett.* **2013**, *110*, 067202.

(5) Jiang, L.; Seok Choi, W.; Jeen, H.; Egami, T.; Lee, H. N. *Appl. Phys. Lett.* **2012**, *101*, 042902.

(6) Zhao, T.; Ogale, S. B.; Shinde, S. R.; Ramesh, R.; Droopad, R.; Yu, J.; Eisenbeiser, K.; Misewich, J. *Appl. Phys. Lett.* **2004**, *84*, 750.

(7) Ahn, C. H.; Triscone, J.-M.; Mannhart, J. *Nature* **2003**, *424*, 1015.

(8) Molegraaf, H. J. A.; Hoffman, J.; Vaz, C. A. F.; Gariglio, S.; van der Marel, D.; Ahn, C. H.; Triscone, J.-M. *Adv. Mater.* **2009**, *21*, 3470.

(9) Vaz, C. A. F.; Hoffman, J.; Segal, Y.; Marshall, M. S. J.; Reiner, J. W.; Zhang, Z.; Grober, R. D.; Walker, F. J.; Ahn, C. H. *J. Appl. Phys.* **2011**, *109*, 07D905.

(10) Lu, H.; George, T. A.; Wang, Y.; Ketsman, I.; Burton, J. D.; Bark, C.-W.; Ryu, S.; Kim, D. J.; Wang, J.; Binek, C.; Dowben, P. A.; Sokolov, A.; Eom, C.-B.; Tsymbal, E. Y.; Gruverman, A. *Appl. Phys. Lett.* **2012**, *100*, 232904.

(11) Dawber, M.; Rabe, K. M.; Scott, J. F. *Rev. Mod. Phys.* **2005**, *77*, 1083.

(12) Meyer, T. L.; Herklotz, A.; Lauter, V.; Freeland, J. W.; Nichols, J.; Guo, E.-J.; Lee, S.; Ward, T. Z.; Balke, N.; Kalinin, S. V.; Fitzsimmons, M. R.; Lee, H. N. *Phys. Rev. B: Condens. Matter Mater. Phys.* **2016**, *94*, 174432.

(13) Lee, H. N.; Nakhmanson, S. M.; Chisholm, M. F.; Christen, H. M.; Rabe, K. M.; Vanderbilt, D. *Phys. Rev. Lett.* **2007**, *98*, 217602.

(14) Goldman, A. *Annu. Rev. Mater. Res.* **2014**, *44*, 45.

(15) Luo, Y.; Li, X.; Chang, L.; Gao, W.; Yuan, G.; Yin, J.; Liu, Z. *AIP Adv.* **2013**, *3*, 122101.

(16) Spurgeon, S. R.; Sloppy, J. D.; Kepaptsoglou, D. M. D.; Balachandran, P. V.; Nejati, S.; Karthik, J.; Damodaran, A. R.; Johnson, C. L.; Ambaye, H.; Goyette, R.; Lauter, V.; Ramasse, Q. M.; Idrobo, J. C.; Lau, K. K. S.; Lofland, E.; Rondinelli, J. M.; Martin, L. W.; Taheri, M. L. *ACS Nano* **2014**, *8*, 894.

(17) Singh, S.; Fitzsimmons, M. R.; Lookman, T.; Thompson, J. D.; Jeen, H.; Biswas, A.; Roldan, M. A.; Varela, M. *Phys. Rev. Lett.* **2012**, *108*, 077207.

(18) Park, J.-H.; Vescovo, E.; Kim, H.-J.; Kwon, C.; Ramesh, R.; Venkatesan, T. *Phys. Rev. Lett.* **1998**, *81*, 1953.

(19) Abad, L.; Martínez, B.; Balcells, L. *Appl. Phys. Lett.* **2005**, *87*, 212502.

(20) Izumi, M.; Ogimoto, Y.; Okimoto, Y.; Manako, T.; Ahmet, P.; Nakajima, K.; Chikyow, T.; Kawasaki, M.; Tokura, Y. *Phys. Rev. B: Condens. Matter Mater. Phys.* **2001**, *64*, 064429.

(21) Huijben, M.; Martin, L. W.; Chu, Y.-H.; Holcomb, M. B.; Yu, P.; Rijnders, G.; Blank, D. H. A.; Ramesh, R. *Phys. Rev. B: Condens. Matter Mater. Phys.* **2008**, *78*, 094413.

(22) Cui, B.; Song, C.; Li, F.; Wang, G. Y.; Mao, H. J.; Peng, J. J.; Zeng, F.; Pan, F. *Sci. Rep.* **2014**, *4*, 4206.

(23) Cui, B.; Song, C.; Wang, G.; Yan, Y.; Peng, J.; Miao, J.; Mao, H.; Li, F.; Chen, C.; Zeng, F.; Pan, F. *Adv. Funct. Mater.* **2014**, *24*, 7233.

(24) Chen, H.; Ismail-Beigi, S. *Phys. Rev. B: Condens. Matter Mater. Phys.* **2012**, *86*, 024433.

(25) Kim, Y.-M.; Morozovska, A.; Eliseev, E.; Oxley, M. P.; Mishra, R.; Selbach, S. M.; Grande, T.; Pantelides, S. T.; Kalinin, S. V.; Borisevich, A. Y. *Nat. Mater.* **2014**, *13*, 1019.

(26) Burton, J. D.; Tsymbal, E. Y. *Phys. Rev. B: Condens. Matter Mater. Phys.* **2009**, *80*, 174406.

(27) Burton, J. D.; Tsymbal, E. Y. *Phys. Rev. Lett.* **2011**, *106*, 157203.

(28) Jiang, L.; Choi, W. S.; Jeen, H.; Dong, S.; Kim, Y.; Han, M.-G.; Zhu, Y.; Kalinin, S. V.; Dagotto, E.; Egami, T.; Lee, H. N. *Nano Lett.* **2013**, *13*, 5837.

(29) Kumar, A.; Barrionuevo, D.; Ortega, N.; Shukla, A. K.; Shannigrahi, S.; Scott, J. F.; Katiyar, R. S. *Appl. Phys. Lett.* **2015**, *106*, 132901.

(30) Zhou, Y.; Park, J.; Shi, J.; Chhowalla, M.; Park, H.; Weitz, D. A.; Ramanathan, S. *Nano Lett.* **2015**, *15*, 1627.

(31) Jeong, J.; Aetukuri, N.; Graf, T.; Schladt, T. D.; Samant, M. G.; Parkin, S. S. P. *Science* **2013**, *339*, 1402.

(32) Altendorf, S. G.; Jeong, J.; Passarello, D.; Aetukuri, N. B.; Samant, M. G.; Parkin, S. S. P. *Adv. Mater.* **2016**, *28*, 5284.

(33) Björck, M.; Andersson, G. *J. Appl. Crystallogr.* **2007**, *40*, 1174.

DOI: 10.1021/acs.nanolett.6b04949
Nano Lett. XXXX, XXX, XXX−XXX